Published OnlineFirst August 31, 2010; DOI: 10.1158/1078-0432.CCR-10-1467

by i.p. injection of 0.15 mL/g body weight of an anesthetic agent, which consisted of dissolved 1.0 g of 2,2,2-tribromoethanol (Wako) in 1.0 mL of 2-methyl-2-butanol (Sigma)/40 mL of H_2O. A median laparotomy was done following disinfection of the abdominal skin. After mobilization of the duodenum, 2×10^6 HT-29/Luc cells suspended in 100 μL of PBS were injected into the portal vein using a Hamilton syringe (30-gauge needle). To prevent either bleeding or dissemination of tumor cells, puncture sites were gently pressed for several minutes. Sterile measures were taken during the operation. All animal procedures were done in compliance with the Guidelines for the Care and Use of Experimental Animals of the National Cancer Center, Japan; these guidelines meet the ethical standards required by law and also comply with the guidelines for the use of experimental animals in Japan.

Bioluminescence imaging

To evaluate and visualize the hepatic metastases of HT-29/Luc cells, *in vivo* bioluminescence imaging was done using the Photon Imager animal imaging system. Mice were i.p. administered D-luciferin potassium salt (Synchem) at 2.5 mg/mouse and anesthetized with isoflurane during imaging. For photon quantification, a region of interest was encircled manually using Photon Vision software (Bio-Space), and the total number of photon per minute [counts per minute (cpm)] was recorded.

In vivo tumor growth inhibition assay

Seven days after the portal injection of HT-29/Luc cells, mice were randomly divided into three test groups consisting of six mice per group (day 0). Randomization was done based on a bioluminescence image (>20,000 cpm), and the mean cpm was confirmed to be statistically identical between groups. The mice were given i.v. injections of 30 mg/kg NK012 and 66.7 mg/kg CPT-11 via the lateral tail vein (200 μL) on days 0, 4, and 8. The dose of NK012 represents the equivalent dose of SN-38 incorporated in the micelle. Control mice were injected with 200 μL of PBS following the same schedule. *In vivo* bioluminescence imaging was done every 7 days from the day of treatment initiation, and the body weight of each mouse was also measured. Mortality and morbidity were checked daily, and the mice were maintained until each mice showed signs of morbidity (massive ascites or observable hepatic tumor, jaundice, and 20% weight loss), at which point they were sacrificed in consideration of animal welfare.

Pharmacokinetics analysis by high-performance liquid chromatography

To assess the biodistribution in each organ, tissue concentrations of NK012, CPT-11, and free SN-38 were measured using high-performance liquid chromatography. Over 14 days after the portal injection of HT-29/Luc cells, female BALB/c nude mice with $>1 \times 10^6$ cpm were used for pharmacokinetics analysis. NK012 (30 mg/kg) or CPT-11 (66.7 mg/kg) was i.v. administered on day 0, as reported (17). After blood removal from the inferior vena cava, the

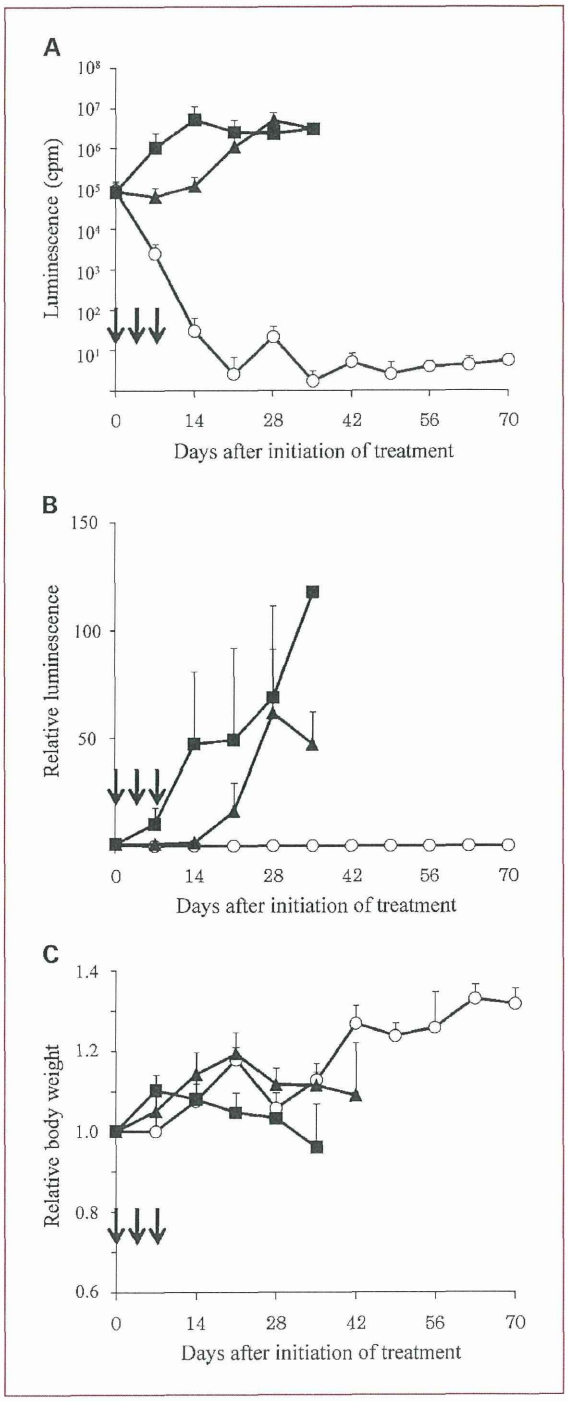

Fig. 1. Effects of NK012 and CPT-11 in HT-29/Luc liver metastasis mouse models. Each treatment was initiated on days 0, 4, and 8 (○, NK012, 30 mg/kg/d, three times; ▲, CPT-11, 66.7 mg/kg/d, three times; ■, control, 200 μL/d, three times). Day 0 indicates 7 d after the portal vein injection of HT-29/Luc cells ($n = 6$). The antitumor activity of NK012 or CPT-11 was evaluated by determining the absolute number (A) and relative number (B) of photon using a Photon Imager system. C, treatment-related body weight loss did not occur in all groups.

Published OnlineFirst August 31, 2010; DOI: 10.1158/1078-0432.CCR-10-1467

metastatic liver tumor, normal liver parenchyma, kidney, and spleen were excised under anesthesia. The analysis time points were 2, 12, 24, 72, 168, 336, 504, 672, and 1,008 hours after NK012 or CPT-11 administration. Pharmacokinetic analysis was conducted using three mice for each time point. The samples were rinsed sufficiently with 0.9% NaCl solution, mixed with 0.1 mol/L glycine-HCl buffer (pH 3.0)/methanol at 5% (w/w), and then homogenized using Precellys 24 (Bertin Technologies). Free SN-38, NK012, and CPT-11 were extracted from each sample, and the extracted sample was analyzed by reversed-phase high-performance liquid chromatography as described previously (17, 19).

Histopathologic analysis

For conventional histopathologic analysis, the liver with a metastatic tumor was excised from the mice bearing liver metastases as described above. The liver was excised after 15 days from the initiation of each treatment and fixed in buffered 4% paraformaldehyde for 72 hours and embedded in paraffin. Then, 3-μm-thick sections were prepared and stained with H&E.

Biodistribution of NK012 as determined by immunohistochemistry and immunofluorescence microscopy

To evaluate the detailed biodistribution of NK012 in immunohistologic sections, we used 20-nm-sized fixable fluorospheres that have equal diameter to NK012 (FluoSpheres, red fluorescent latex microspheres; Molecular Probes) as a reference of positional relationship within the tissue. Because NK012 could neither be fixed nor stained with other antibodies, we applied this fluorescent-labeled macromolecular substance whose surface is carboxylate modified to decrease nonspecific binding. Five minutes after NK012 administration (30 mg/kg) to mice with liver metastases, fluorospheres (0.25 mL/animal; concentration, 2.5 mg/mL) were also injected i.v. The mice were sacrificed under deep anesthesia and perfused with 0.9% NaCl through the inferior vena cava to prevent blood stasis, and then the liver with metastases was excised 2 hours and 1, 3, and 7 days from the administration of NK012 and fluorospheres. The samples were embedded in an OCT compound (Sakura Finetechnochemical) and quickly frozen in liquid nitrogen.

For direct observation of the fluorescence of NK012 and fluorospheres, 10-μm-thick frozen sections were prepared using a cryostat and examined under a fluorescence microscope (BIOREVO BZ9000; Keyence) at an excitation wavelength of 377 nm and an emission wavelength of 447 nm to evaluate NK012 distribution. For immunohistochemical analysis, frozen sections were prepared as described earlier and fixed in 4% paraformaldehyde in PBS (pH 7.4). After blocking, sections were incubated for 1 hour at room temperature with primary antibodies. Anti-CD31 goat antibody for endothelial cells (R&D Systems) was used at 1:200 dilution, and anti-CD68 rat antibody for macrophages (Kupffer cells; AbD Serotec) was used at 1:200 dilution. The sections were then incubated with the following secondary antibodies at 1:500 dilution: Alexa 647 donkey anti-goat IgG, Alexa 488 goat anti-rat IgG, or Alexa 647 goat anti-rat IgG. Nuclei were

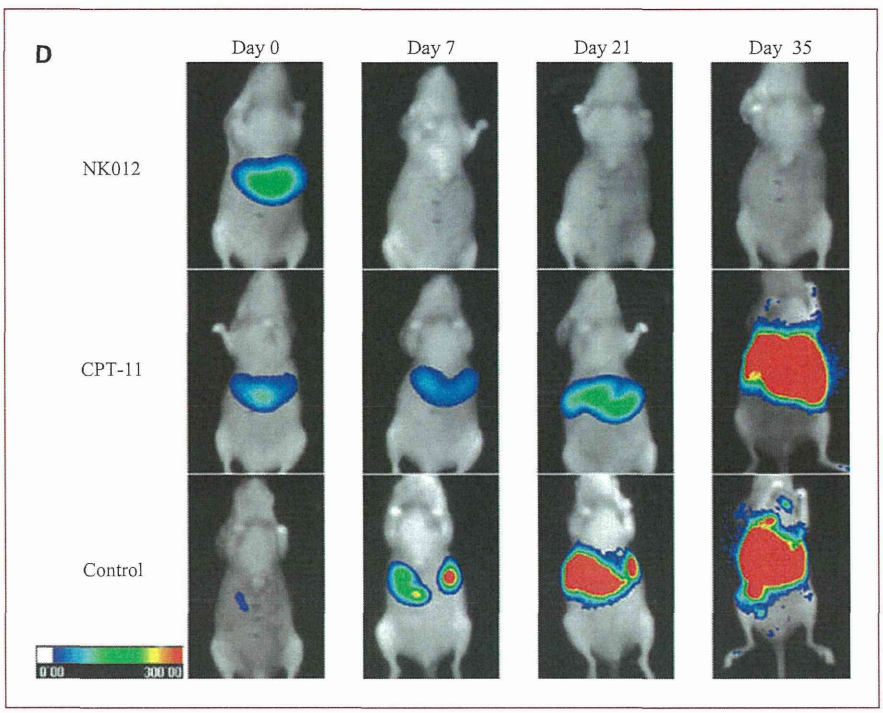

Fig. 1. *Continued.* D, images of an HT-29/Luc mouse model treated with each regimen taken using a Photon Imager system on days 0, 7, 21, and 35 after therapy initiation. Points, mean; bars, SD. Arrows, drug injections. Statistical comparisons between the NK012 group and the CPT-11 group were done by ANOVA on day 28 after treatment initiation ($P < 0.0001$).

Published OnlineFirst August 31, 2010; DOI: 10.1158/1078-0432.CCR-10-1467

counterstained with 4′,6-diamidino-2-phenylindole at 1:1,000 dilution (Roche).

Statistical analysis

Data were expressed as mean ± SD. To evaluate changes in the photon count of each treatment group, repeated-measures ANOVA was used. Survival was assessed using the Kaplan-Meier method. For all tests, P values of <0.05 were considered significant using SPSS software version 12.0 (SPSS, Inc.). All statistical tests were two-sided.

Results

Antitumor activity of NK012 and CPT-11 against HT-29/Luc liver metastasis model

Comparison of the relative photon count on day 28 in the HT-29/Luc liver metastasis model revealed significant differences between mice given NK012 and those given CPT-11 (P = 0.002; Fig. 1A, B, and D). The survival rates on day 140 in the three test groups were 100%, 0%, and 0% for the NK012, CPT-11, and control groups, respectively (Fig. 2). Moreover, neither relapse nor any other clinical problems were observed in the NK012 group until day 140. Kaplan-Meier analysis showed that a significant improvement in the survival rate was observed in the NK012 group compared with the CPT-11 group (P = 0.0006), whereas there was no significant improvement between the CPT-11 group and the control group (P = 0.1556). There was no severe body weight loss or toxic death for any treatment used in this study (Fig. 1C).

Histopathologic findings

Histopathologic observation of liver metastases after NK012 administration showed the disappearance of tumor cells. Tumor tissue was replaced with fibrotic or granulomatous tissue with mild infiltration of inflammatory cells. On the other hand, liver metastases treated with CPT-11 showed slight degeneration of cancer cells and few apoptotic cells (Fig. 3). At the liver parenchyma, sinusoidal dilation or steatosis that was a characteristic feature of chemotherapy-associated liver toxicity was not observed after a single or triple administration of NK012.

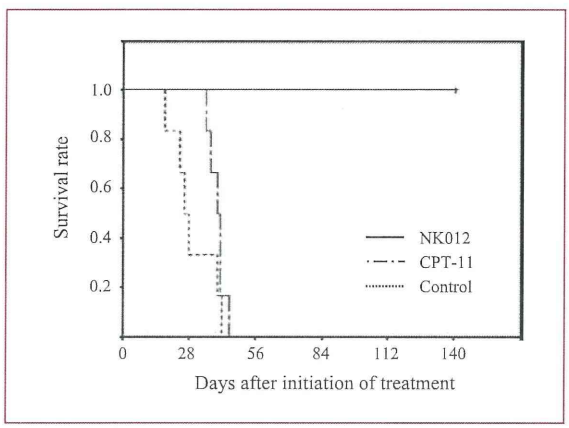

Fig. 2. Kaplan-Meier curves of HT-29/Luc liver metastasis models. The NK012 group (30 mg/kg/d), CPT-11 group (66.7 mg/kg/d), and control group (PBS, 200 μL/d) were administered each drug on days 0, 4, and 8 (n = 6). Treatment was initiated 7 d after the portal injection of HT-29/Luc cells. Log-rank test: NK012 group versus CPT-11 group, P = 0.0006; CPT-11 group versus control group, P = 0.1556.

Tissue concentration and transition of SN-38 after NK012 and CPT-11 administration

We investigated the concentration-time profile of NK012, CPT-11, and free SN-38 in various tissues after single i.v. administration more precisely compared with a previous report (17). The accumulation of free SN-38 converted from CPT-11 was rapidly decreased within 24 hours and could not be detected thereafter in the plasma (Fig. 4A), liver, spleen, kidney, and liver tumor (Fig. 4B). In contrast, the accumulation of free SN-38 released by NK012 was maintained at a relatively high level for weeks after administration. Notably, prolonged higher accumulation of free SN-38 and NK012 was observed in the liver and spleen, which are organs categorized under the reticuloendothelial system. The concentrations of free SN-38 and NK012 gradually decreased over 6 weeks.

Biodistribution of NK012 in hepatic metastases and liver parenchyma

First, we observed directly the distribution and relationship of NK012 and fluorospheres to confirm the detailed biodistribution of NK012 in tissue. In the metastatic tumor, the biodistribution of both substances was similar after 24 hours following their administration, whereas a discrepancy was found at 2 hours (Fig. 5A). For the normal liver parenchyma, fluorescence microscopy showed a similar biodistribution of NK012 and fluorospheres with the exception of the weak accumulation of NK012 2 hours after administration (Fig. 5B).

Second, we observed fluorospheres as a reference of NK012 distribution by immunohistochemistry. Anti-CD31 and anti-CD68 antibodies were used as vascular endothelial cell and macrophage (Kupffer) cell markers, respectively. Fluorospheres distributed around tumor vessels in the metastatic liver tumor in all observation points (Fig. 6A). For the liver parenchyma, fluorospheres were not observed in the hepatocytes but were well phagocytized by CD68-positive Kupffer cells in all observation points (Fig. 6B). In addition, the number of CD68-positive cells did not decrease significantly (data not shown).

Discussion

This study highlights four novel findings. First, NK012 was strongly effective in mice bearing liver metastases of human colorectal cancer cells. Second, free SN-38 released from NK012 showed high accumulation and NK012 was detected in the liver metastatic tumor for a long time. Third, free SN-38 and NK012 had been retained in the liver and spleen for weeks with no accompanying toxicity to normal

Published OnlineFirst August 31, 2010; DOI: 10.1158/1078-0432.CCR-10-1467

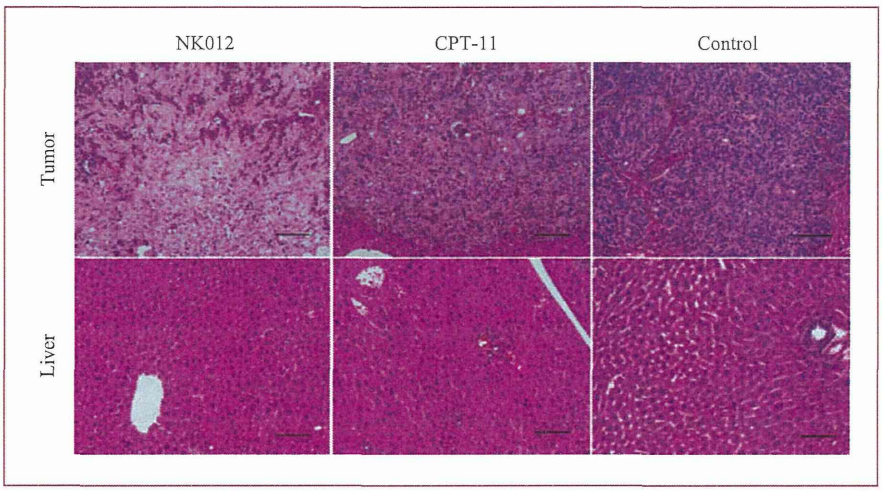

Fig. 3. H&E-stained sections of metastatic tumor and liver treated with NK012 and CPT-11. Scale bars, 100 μm. NK012 (30 mg/kg/d), CPT-11 (66.7 mg/kg/d), and PBS (200 μL/d) were administered on days 0, 4, and 8 following the same schedule as the treatment studies. Metastatic tumors and livers were excised on day 15 after treatment initiation.

organs either symptomatically or pathologically. Fourth, NK012 entrapment by macrophages in the liver and spleen led to its prolonged accumulation, and NK012 retention around tumor vessels also resulted in its relatively high accumulation lasting for weeks.

To our knowledge, this is the first study to show that NK012 completely eradicated orthotopic tumors in an orthotopic model, in addition to our previously reported potent antitumor effects of NK012 against various models using human cancer cell lines (17–20, 25). The strong antitumor activity of NK012 is attributable to the high concentration of free SN-38 released from NK012 in the tumor, which is higher than any other concentrations previously reported. Liver metastasis in a specific organ has an adequate potential to be a target of DDS agents, although it presents a disadvantage for such agents because it is considered a hypovascular tumor.

The accumulation and metabolism of DDS agents are closely associated with their biodistribution. The two major differences about the distribution between NK012 and fluorospheres 2 hours after administration in direct fluorescence observation are the lower accumulation of NK012 in the liver parenchyma and discrepancy in metastatic liver tumor (Fig. 5A and B). In agreement with previous reports, these data indicate that NK012 extravasation was successfully achieved and NK012 uptake by Kupffer cells was less than fluorosphere uptake during the early phase after administration because of the higher biocompatibility of the outer shell, which was enveloped by polyethyleneglycol (26–28). NK012 biodistribution was similar to fluorosphere biodistribution after 24 hours following administration, and therefore, this fixable fluorescence-labeled nanoparticle can be considered as a substitute for NK012 observation in histochemical studies after such period. Considering these facts, NK012 was retained around CD31-positive tumor vessels in the metastatic tumors and stored in CD68-positive macrophage cells in the liver parenchyma during the late phase after administration, thereby resulting in the high concentration of free SN-38 in the tumor and liver for weeks.

The metabolic pathway of NK012 also plays an important role in organ toxicities. Specifically, the mechanism of liver injury has not yet been clarified, but it is speculated that mitochondrial damage due to cytotoxic agents and the resulting reactive oxygen species have some effect on liver toxicities (29). As for NK012 and CPT-11, SN-38 is detoxified mainly in normal liver cells to form SN-38 β-glucuronide (inactive form) by UDP-glucuronosyltransferase, and the detoxification capability may be related to liver toxicities (30). In this study, the single or triple administration of NK012 at the maximum tolerable dose showed no chemotherapy-associated liver toxicity in terms of pathologic changes (Fig. 3) and blood biochemical findings, which reflects hepatocyte injury (data not shown). Daemen et al. (31) reported severe depletion of liver macrophages 24 hours after the administration of liposomal doxorubicin and emphasized the possibility of developing infection due to depletion of the phagocytic capacity of the reticuloendothelial system. Notably, our present data are not in agreement with those of Daemen et al. The number of CD68-positive cells did not decrease because NK012, which is endocytosed in Kupffer cells, is rapidly transported to an acidic environment (pH <5.0), and this novel polymeric micelle agent is very stable at such an acidic condition, indicating that NK012 gradually releases free SN-38 after it accumulates in Kupffer cells (17, 32). Given the metabolite pathway of SN-38 and present data, NK012 causes neither injury of hepatocytes nor depletion of Kupffer cells. However, further studies of liver toxicity with repeated NK012 administrations and the detoxification capability of SN-38, which is gradually released from NK012 for a long period, are needed to clarify whether the prolonged use of NK012 causes chemotherapy-associated liver toxicity or not.

A limitation of this study is the difficulty in the observation of NK012 or free SN-38 by fluorescence microscopy to show their detailed biodistribution. This is because

Published OnlineFirst August 31, 2010; DOI: 10.1158/1078-0432.CCR-10-1467

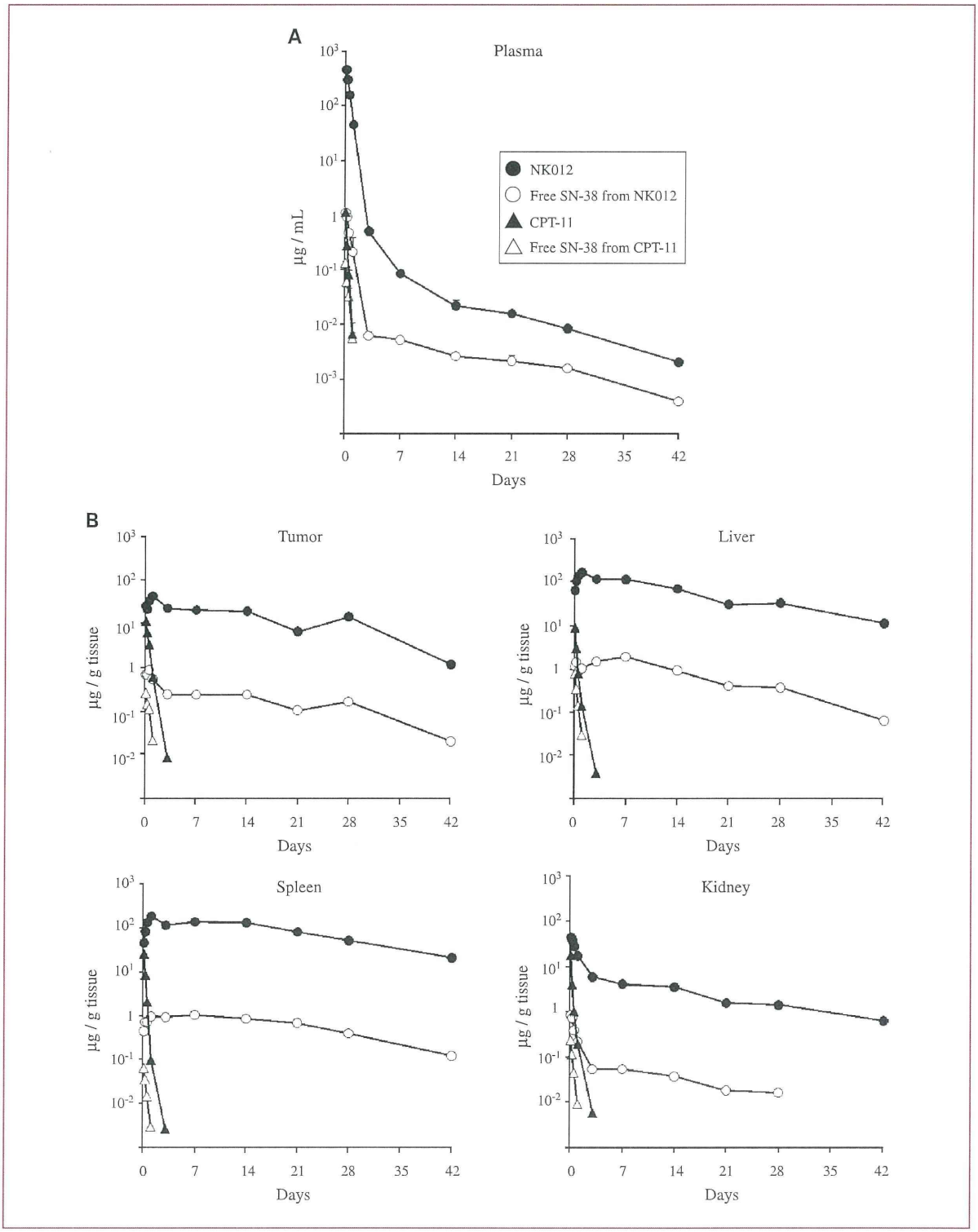

Fig. 4. Transition of plasma and tissue concentration after single administration of NK012 (30 mg/kg) or CPT-11 (66.7 mg/kg) to HT-29/Luc liver metastasis mouse models (n = 3). A, plasma. B, tissue. ●, NK012; ○, free SN-38 released from NK012; ▲, CPT-11; △, free SN-38 converted from CPT-11. Points, mean; bars, SD. Arrows, drug injections.

Published OnlineFirst August 31, 2010; DOI: 10.1158/1078-0432.CCR-10-1467

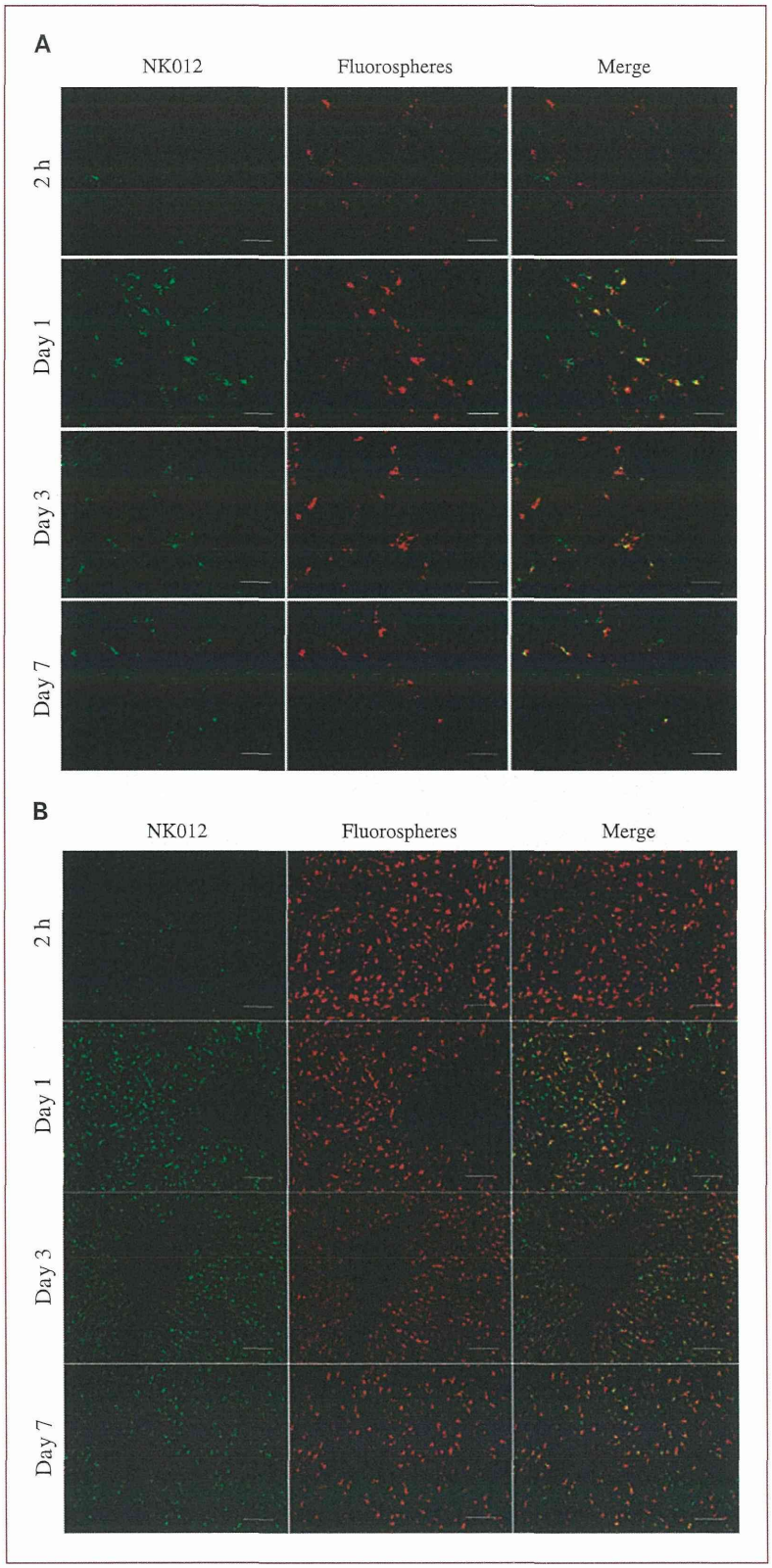

Fig. 5. Biodistribution of NK012 and fluorospheres in hepatic metastasis and liver parenchyma for assessment of distributional relationship of the two substances. Frozen sections of livers from HT-29/Luc liver metastasis nude mice administered NK012 and fluorospheres were directly observed by fluorescence microscopy. A, liver metastatic tumor. Scale bars, 50 μm. B, liver parenchyma. Scale bars, 100 μm.

Published OnlineFirst August 31, 2010; DOI: 10.1158/1078-0432.CCR-10-1467

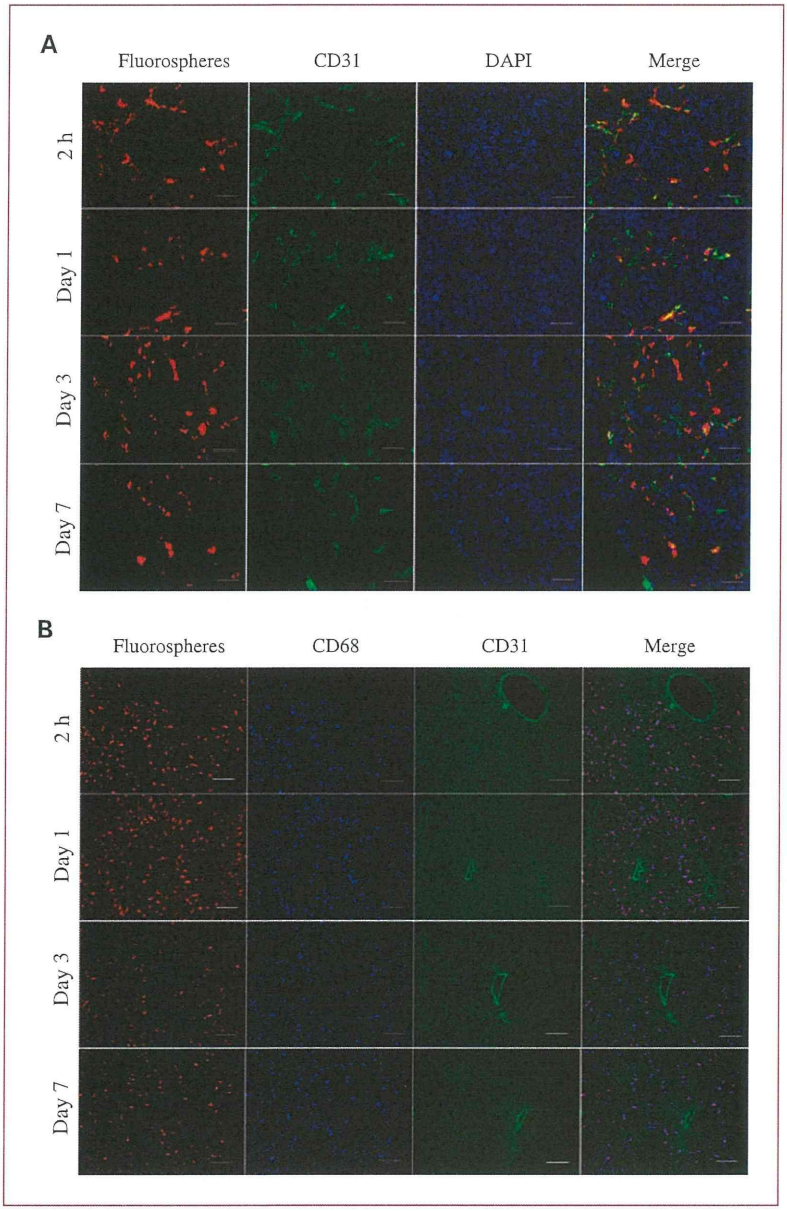

Fig. 6. Immunohistochemical analysis to assess fluorosphere distribution as criteria of NK012 biodistribution. Frozen sections of livers from HT-29/Luc liver metastasis nude mice administered NK012 and fluorospheres were stained immunohistochemically followed by fluorescence microscopy observations. A, liver metastatic tumor. Scale bars, 50 μm. B, liver parenchyma. Scale bars, 100 μm.

NK012 cannot be fixed and the fluorescence intensities of NK012 and free SN-38 are very weak. Here, we used 20-nm-sized fixable fluorospheres as a substitute for NK012, although direct observation of the object substance remains the best method to verify NK012 biodistribution. There is, however, a technical difficulty in developing a fixable fluorescence substance with entirely the same properties as those of developed DDS agents.

CPT-11 has been approved for the treatment of advanced colorectal cancer in combination with other agents such as fluorouracil, leucovorin, and molecular targeting agents. However, the intensive use of CPT-11 induces chemotherapy-associated steatohepatitis, which affects mortality or morbidity of hepatectomy. NK012 is a biocompatible agent for the treatment of CLM and an excellent SN-38 vehicle because SN-38 is a time-dependent anticancer agent, and the appropriate SN-38 concentration released by NK012 is well maintained for a long time in liver metastases. In terms of liver toxicity, NK012 seems to be nontoxic as shown in this study regardless of the long-term storage of NK012 in Kupffer cells.

In conclusion, NK012 showed strong antitumor effects against liver metastatic tumor. NK012 well infiltrates metastatic tumor tissue and cannot be easily endocytosed by

Published OnlineFirst August 31, 2010; DOI: 10.1158/1078-0432.CCR-10-1467

macrophages during the early phase after administration. The excellent biodistribution and metabolite pathway of NK012 corroborates both its strong antitumor effects and low toxicity. Our data warrant clinical evaluation of NK012 for the treatment of liver metastases of colorectal cancer.

Disclosure of Potential Conflicts of Interest

No potential conflicts of interest were disclosed.

Acknowledgments

A. Takahashi would like to thank the Foundation for Promotion of Cancer Research (Japan) for the Third-Term Comprehensive Control Research for Cancer for awarding him a research resident fellowship. We thank N. Mie and M. Ohtsu for technical assistance and K. Shiina and K. Abe for secretarial assistance.

Grant Support

Grant-in-Aid for Third-Term Comprehensive Control Research for Cancer from the Ministry of Health, Labour and Welfare of Japan (Y. Matsumura); Scientific Research on Priority Areas grant 17016087 from the Ministry of Education, Culture, Sports, Science and Technology (Y. Matsumura); Japanese Foundation for Multidisciplinary Treatment of Cancer (Y. Matsumura); and Princess Takamatsu Cancer Research Fund grant 07-23908.

The costs of publication of this article were defrayed in part by the payment of page charges. This article must therefore be hereby marked *advertisement* in accordance with 18 U.S.C. Section 1734 solely to indicate this fact.

Received 05/31/2010; revised 08/15/2010; accepted 08/18/2010.

References

1. Scheele J, Stang R, Altendorf-Hofmann A, Paul M. Resection of colorectal liver metastases. World J Surg 1995;19:59–71.
2. Steele G, Jr., Ravikumar TS. Resection of hepatic metastases from colorectal cancer. Biologic perspective. Ann Surg 1989;210:127–38.
3. Bismuth H, Adam R, Levi F, et al. Resection of nonresectable liver metastases from colorectal cancer after neoadjuvant chemotherapy. Ann Surg 1996;224:509–20.
4. Adam R, Delvart V, Pascal G, et al. Rescue surgery for unresectable colorectal liver metastases downstaged by chemotherapy: a model to predict long-term survival. Ann Surg 2004;240:644–57.
5. Hurwitz H, Fehrenbacher L, Novotny W, et al. Bevacizumab plus irinotecan, fluorouracil, and leucovorin for metastatic colorectal cancer. N Engl J Med 2004;350:2335–42.
6. Diaz-Rubio E, Tabernero J, Gomez-Espana A, et al. Phase III study of capecitabine plus oxaliplatin compared with continuous-infusion fluorouracil plus oxaliplatin as first-line therapy in metastatic colorectal cancer: final report of the Spanish Cooperative Group for the Treatment of Digestive Tumors Trial. J Clin Oncol 2007;25:4224–30.
7. Fernandez FG, Ritter J, Goodwin JW, Linehan DC, Hawkins WG, Strasberg SM. Effect of steatohepatitis associated with irinotecan or oxaliplatin pretreatment on resectability of hepatic colorectal metastases. J Am Coll Surg 2005;200:845–53.
8. Rubbia-Brandt L, Audard V, Sartoretti P, et al. Severe hepatic sinusoidal obstruction associated with oxaliplatin-based chemotherapy in patients with metastatic colorectal cancer. Ann Oncol 2004;15:460–6.
9. Karoui M, Penna C, Amin-Hashem M, et al. Influence of preoperative chemotherapy on the risk of major hepatectomy for colorectal liver metastases. Ann Surg 2006;243:1–7.
10. Aloia T, Sebagh M, Plasse M, et al. Liver histology and surgical outcomes after preoperative chemotherapy with fluorouracil plus oxaliplatin in colorectal cancer liver metastases. J Clin Oncol 2006; 24:4983–90.
11. Kopetz S, Hoff PM, Morris JS, et al. Phase II trial of infusional fluorouracil, irinotecan, and bevacizumab for metastatic colorectal cancer: efficacy and circulating angiogenic biomarkers associated with therapeutic resistance. J Clin Oncol 28:453–9.
12. Reddy SK, Morse MA, Hurwitz HI, et al. Addition of bevacizumab to irinotecan- and oxaliplatin-based preoperative chemotherapy regimens does not increase morbidity after resection of colorectal liver metastases. J Am Coll Surg 2008;206:96–106.
13. Mathijssen RH, van Alphen RJ, Verweij J, et al. Clinical pharmacokinetics and metabolism of irinotecan (CPT-11). Clin Cancer Res 2001; 7:2182–94.
14. Slatter JG, Schaaf LJ, Sams JP, et al. Pharmacokinetics, metabolism, and excretion of irinotecan (CPT-11) following I.V. infusion of [14C] CPT-11 in cancer patients. Drug Metab Dispos 2000;28:423–33.
15. Rothenberg ML, Kuhn JG, Burris HA III, et al. Phase I and pharmacokinetic trial of weekly CPT-11. J Clin Oncol 1993;11:2194–204.
16. Matsumura Y, Maeda H. A new concept for macromolecular therapeutics in cancer chemotherapy: mechanism of tumoritropic accumulation of proteins and the antitumor agent smancs. Cancer Res 1986;46:6387–92.
17. Koizumi F, Kitagawa M, Negishi T, et al. Novel SN-38-incorporating polymeric micelles, NK012, eradicate vascular endothelial growth factor-secreting bulky tumors. Cancer Res 2006;66:10048–56.
18. Sumitomo M, Koizumi F, Asano T, et al. Novel SN-38-incorporated polymeric micelle, NK012, strongly suppresses renal cancer progression. Cancer Res 2008;68:1631–5.
19. Kuroda J, Kuratsu J, Yasunaga M, Koga Y, Saito Y, Matsumura Y. Potent antitumor effect of SN-38-incorporating polymeric micelle, NK012, against malignant glioma. Int J Cancer 2009;124:2505–11.
20. Nakajima TE, Yanagihara K, Takigahira M, et al. Antitumor effect of SN-38-releasing polymeric micelles, NK012, on spontaneous peritoneal metastases from orthotopic gastric cancer in mice compared with irinotecan. Cancer Res 2008;68:9318–22.
21. Alexis F, Pridgen E, Molnar LK, Farokhzad OC. Factors affecting the clearance and biodistribution of polymeric nanoparticles. Mol Pharmacol 2008;5:505–15.
22. Lee MJ, Veiseh O, Bhattarai N, et al. Rapid pharmacokinetic and biodistribution studies using cholorotoxin-conjugated iron oxide nanoparticles: a novel non-radioactive method. PLoS One 5:e9536.
23. Peer D, Karp JM, Hong S, Farokhzad OC, Margalit R, Langer R. Nanocarriers as an emerging platform for cancer therapy. Nat Nanotechnol 2007;2:751–60.
24. Zamboni WC. Liposomal, nanoparticle, and conjugated formulations of anticancer agents. Clin Cancer Res 2005;11:8230–4.
25. Kuroda J, Kuratsu J, Yasunaga M, et al. Antitumor effect of NK012, a 7-ethyl-10-hydroxycamptothecin-incorporating polymeric micelle, on U87MG orthotopic glioblastoma in mice compared with irinotecan hydrochloride in combination with bevacizumab. Clin Cancer Res 16:521–9.
26. Allen TM, Cullis PR. Drug delivery systems: entering the mainstream. Science 2004;303:1818–22.
27. Duncan R. The dawning era of polymer therapeutics. Nat Rev Drug Discov 2003;2:347–60.
28. Gabizon AA. Stealth liposomes and tumor targeting: one step further in the quest for the magic bullet. Clin Cancer Res 2001;7:223–5.
29. Chun YS, Laurent A, Maru D, Vauthey JN. Management of chemotherapy-associated hepatotoxicity in colorectal liver metastases. Lancet Oncol 2009;10:278–86.
30. Rouits E, Charasson V, Petain A, et al. Pharmacokinetic and pharmacogenetic determinants of the activity and toxicity of irinotecan in metastatic colorectal cancer patients. Br J Cancer 2008;99:1239–45.
31. Daemen T, Hofstede G, Ten Kate MT, Bakker-Woudenberg IA, Scherphof GL. Liposomal doxorubicin-induced toxicity: depletion and impairment of phagocytic activity of liver macrophages. Int J Cancer 1995;61:716–21.
32. Schreiber R, Zhang F, Haussinger D. Regulation of vesicular pH in liver macrophages and parenchymal cells by ammonia and anisotonicity as assessed by fluorescein isothiocyanate-dextran fluorescence. Biochem J 1996;315:385–92.

RESEARCH ARTICLE

SPECIAL FOCUS: ONCOLOGY

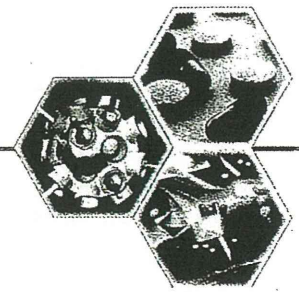

Optimum conditions of ultrasound-mediated destruction of bubble liposome for siRNA transfer in bladder cancer

Background: We investigated the effectiveness of ultrasound-mediated destruction of bubble liposome (UBL) for siRNA transfer by observing reduction in the luciferase activity of human bladder tumor RT-112 cells transfected with the luciferase gene (*RT-112Luc*) following luciferase siRNA transfer into the cells. **Results:** siRNA was transferred to 26% of RT-112Luc cells by UBL and the luciferase activity of RT-112Luc cells was significantly suppressed by UBL using the luciferase siRNA, compared with that using nonspecific siRNA *in vitro* ($p = 0.036$). The luciferase activity of RT-112Luc tumor was suppressed by UBL using luciferase siRNA compared with that using nonspecific siRNA 2 days after the *in vivo* treatment. **Conclusion:** This study showed that UBL is suitable for siRNA transfer to mammalian cells.

Bladder cancer is classified into two types, superficial and invasive. In clinics, 70% of bladder cancers are reported to be the superficial type, which does not invade the muscle layer of the bladder wall [1]. The standard treatment of superficial bladder cancers is transurethral resection of the bladder cancer followed by the intravesical instillation of an anticancer drug or Bacillus Calmette–Guerin (BCG) to prevent tumor recurrence.

However, in half of surgically treated patients, bladder tumors recur and 10–30% of recurrent bladder tumors become invasive. Patients with an invasive tumor inevitably undergo radical cystectomy. Moreover, subsidiary BCG treatment usually causes unbearable cystitis manifested with fever and local pain [2]. Therefore, a new modality that results in good quality of life and prevents the recurrence of the superficial bladder tumor is urgently needed.

siRNA is a sequence-specific double-strand RNA and has been newly recognized as a powerful and useful tool for gene expression inhibition [3,4]. The RNAi effect on the cytosol is transient and the 'off or on' of the treatment can be readily controlled [5]. When side effects induced by RNAi occur, treatment can be stopped before the occurrence of serious side effects. As sequence-specific siRNA can be prepared exquisitely using sequence information, RNAi therapy may have the possibility to be a new, convenient and safe modality in clinics. Recently, the intravesical application of RNAi targeting PLK-1 in a mice bladder cancer model using cationic liposome has been reported as a new therapy for bladder cancer [6]. Furthermore, plasmid DNA transfection [7–13] and siRNA [13–18] to cells using sonoporation, combined with ultrasound (US) and microbubble has been reported. Microbubble has been demonstrated to collapse by US irradiation; transient permeability of the cell membrane occurred by the cavitation following the destruction of microbubble and finally the plasmid DNA was transfected to the cells efficiently [19–21].

Previously, we developed a novel liposomal bubble (bubble liposome [BL]) that encapsulated the perfluoropropane nanobubble in the lipid bilayer [22]. The mean size of the BLs was approximately 800–900 nm, which is smaller than microbubbles used for ultrasound imaging such as Sonazoid™, Optison™ and SonoVue® [23,24]. BLs may be useful for local or systemic delivery of a gene to the target site (cancer tissue) followed by ultrasound exposure to the site for transferring the gene to cancer cells [25].

In this context, we have investigated a new method of siRNA transfection *in vitro* and *in vivo* using ultrasound-mediated destruction of BL.

Experimental

■ Cell line

The human bladder tumor cell line RT-112 was purchased from the American Type Culture Collection (VA, USA). For the *in vitro* experiments and *in vivo* bioluminescence imaging of

Suguru Fujisawa[1,4], Hiroshige Arakawa[1,4], Ryo Suzuki[2], Kazuo Maruyama[2], Tetsuya Kodama[3], Masahiro Yasunaga[4], Yoshikatsu Koga[4] & Yasuhiro Matsumura†[4]

[1]Graduate School of Frontier Science, The University of Tokyo, Japan
[2]School of Pharmaceutical Sciences, Teikyo University, Japan
[3]Graduate School of Biomedical Engineering, Tohoku University, Japan
[4]Investigative Treatment Division, Research Center for Innovative Oncology, National Cancer Center Hospital East, 6–5–1 Kashiwanoha, Kashiwa-City, Chiba 277–8577, Japan
†Author for correspondence:
Tel.: +81 4 7134 6857
Fax: +81 4 7134 6866
E-mail: yhmatsum@east.ncc.go.jp

FUTURE SCIENCE part of fsg

subcutaneous tumors, the RT-112 cell line stably expressing firefly luciferase and the YFP mutant Venus RT-112^{Luc} was established. In brief, the coding sequence for firefly luciferase and Venus was subcloned into the pIRES Vector (Clontech Laboratories, CA, USA). The fragment consists of Luciferase-IRES-Venus generated from the plasmid with the restriction enzymes NheI and NotI. This fragment was subcloned into the pEF6/V5-His Vector (Invitrogen, CA, USA) to generate plasmids of pEF6-Luciferase IRES Venus. RT-112 cells were seeded onto 1/6-well plate, 24 h before the transfection. The cells were transfected with pEF6-Luciferase IRES Venus (2 µg) using FuGENE HD transfection reagent (Roche Diagnostics, Mannheim, Germany) according to manufacturer's instructions, and then incubated for 48 h at 37°C. The cells were then passaged in medium containing Blasticidin (10 µg/ml; InvivoGen, CA, USA) to select for the blasticidin-resistance gene integrated in the pEF6/V5-His plasmids. Venus expression was used as a surrogate marker of luciferase-positive RT-112^{Luc}. RT-112^{Luc} cells were sorted using the BD FACS Aria cell sorter (BD Biosciences, CA, USA) and expanded in selection medium. RT-112 and RT-112^{Luc} were grown in Dulbecco's Modified Eagle's Medium (Wako, Tokyo, Japan) containing 10% fetal bovine serum (Tissue Culture Biologicals, CA, USA), 2 mM L-glutamine (Sigma-Aldrich, MO, USA), 100 U/ml penicillin, 100 µg/ml streptomycin and 0.25 µg/ml amphotericin B (100 × antibiotic–antimycotic, GIBCO, CA, USA) in a humidified atmosphere at 37°C and 5% CO_2.

■ US irradiation

The intensity of the US probe (BFC applications, Fujisawa, Japan) used in this study was calibrated using a hydrophone (ONDA, CA, USA) in a water bath. The probe was immersed in the water bath at 0.5 cm from the water surface. The cells were plated in a cell culture plate and mice were immersed in water and irradiated using US.

■ Bubble liposome

Liposomes composed of 1,2-distearoyl-sn-glycero-3-phosphocholine (DSPC, NOF corporation, Tokyo, Japan) and *N*-(carbonyl-methoxypolyethyleneglycol 2000)-1,2-distearoyl-sn-glycero-3-phosphoethanolamine (DSPE-PEG(2k)-OMe, NOF corporation) (94:6 m/m) were prepared by reverse-phase evaporation. In brief, all reagents were dissolved in 1:1 (v/v) chloroform/diisopropyl ether and then 4 ml of phosphate buffered saline (PBS, Invitrogen) was added. The mixture was sonicated and evaporated at 65°C. The solvent was completely removed, and the size of the liposomes was adjusted to less than 200 nm using an extruding apparatus (Northern Lipids Inc., BC, Canada) and sizing filters (pore sizes: 100 and 200 nm; Nuclepore Track-Etch Membrane, Whatman PLC, UK). After sizing, the liposomes were sterilized by passing them through a 0.45-µm pore size filter (MILLEX HV filter unit, Durapore PVDF membrane, Millipore Corporation, MA, USA). BLs were prepared from the liposomes and perfluoropropane gas (Suganuma Sangyo, Tokyo, Japan) [23,26,27]. In brief, 2 ml of 1 mg/ml liposome in PBS was poured into a 5-ml vial (As One, Osaka, Japan). The vial was tightly covered, followed by the addition of 7.5 ml of perfluoropropane gas. To prepare BLs, the vial was shaken vigorously for a few minutes in the Ultra sonic cleaner vs-100 (As One). Being unstable, the BL should be used within 10 min (data not shown).

■ Optimum conditions of UBL *in vitro*

To determine the optimum conditions of UBL, fluorescein isothiocyanate (FITC)-dextran internalization was analyzed by flow cytometry using FACS Calibur (BD Biosciences). RT-112 cells (6.0×10^5) and 500 nM (final concentration) 10 kDa FITC-dextran (Invitrogen) were mixed in flat-bottomed 48-well cell-culture plates (NY, USA) and treated using several conditions of UBL. The US and BL conditions used in this simulation study were as follows; US intensity: 1, 2, 3 or 4 W/cm^2; duration of US irradiation: 10, 30 or 50 s; final concentration of the BL: 0.1, 0.2 or 0.3 mg/ml; interval time of US irradiation after addition of the BL: 15, 30, 60 or 300 s.

At 24 h after the treatment, surviving cells were trypsinized and resuspended in PBS containing 0.5% bovine serum albumin and 2 mM EDTA and FITC-positive cells were analyzed by flow cytometry. FITC-positive cells were defined by comparison of the cells without the treatment as negative control in the gating area of living cells (propidium iodide exclusion method) using flow cytometry.

Cytotoxic effect was also analyzed under the several conditions of UBL. RT-112 cells were treated using the same conditions as described